Dislocation Distribution and Prediction of Fatigue Damage

R. N. PANGBORN, S. WEISSMANN, AND I. R. KRAMER

The dislocation density and distribution induced by tensile deformation in single crystals of silicon, aluminum and gold and by tension-compression cycling in aluminum single crystals and Al 2024-T3 alloys were studied by X-ray double-crystal diffractometry. The measurements of dislocation density were made at various depths from the surface by removing surface layers incrementally. In this way, a propensity for work hardening in the surface layers compared to the bulk material was demonstrated for both tensile-deformed and fatigue-cycled metals. Analysis of the cycled Al 2024 alloy as a function of the fraction of fatigue life showed that the dislocation density in the surface layer increased rapidly early in the fatigue life and maintained virtually a plateau value from 20 to 90 pct of the life. Beyond 90 pct the dislocation density increased rapidly again to a critical value at failure. Evaluation of the dislocation distribution in depth showed that the excess dislocation density in the bulk material increased more gradually during the life. Using deeply penetrating molybdenum K_α radiation, capable of analyzing grains representative of the bulk region, the accrued damage and the onset of fatigue failure could be predicted nondestructively for 2024 Al, cycled with constant stress as well as with variable stress amplitude. The dislocation structure produced in the bulk by prior cycling was unstable when the work-hardened surface layer was removed. It is proposed that the deformation response of the bulk material is controlled by the accumulation of dislocations and associated stresses in the surface layer.

1. INTRODUCTION

A RELIABLE and practical means for forecasting fatigue failure through the measurement of accumulated damage has been sought for many years. Despite the considerable effort devoted to nondestructive evaluation of fatigue damage, however, only limited progress has been made toward correlating the cumulative damage to the amount of fatigue life actually expended. Since X-ray diffraction analysis provides a sensitive indication of structural changes due to deformation, a variety of diffraction methods has been applied to study fatigued metals and alloys.[1] Many investigators have reported changes in the X-ray patterns during the early stages of cycling, including the appearance of asterism, line shifts and peak broadening.[2-8] For much of the subsequent fatigue life, however, the diffraction patterns were found to remain virtually unaltered, until the initiation of macroscopic failure. As a result of the invariance of the X-ray patterns during a very long period of cycling, from approximately 20 to 90 pct of the life, attempts to predict failure from any stage prior to the terminal one were unsuccessful.

The current study was focused on achieving two primary goals: 1) to identify the differences in deformation response between the surface layer and bulk material for both single and polycrystalline metals, by determining the dislocation density and distribution at various depths into the sample, and 2) to provide an assessment of the localized deformation incurred by the individual grains of a fatigued alloy, and at the same time, to evaluate the overall, average fatigue damage in the surface and bulk regions, respectively.

The first objective derived from a number of previous investigations which had indicated that when a metal is stressed, a surface layer that extends about 100 to 300 μm in depth work hardens to a greater extent than the bulk material.[9-12] High resolution stress-strain analysis, etch pit density measurements and transmission electron microscopy were employed to provide evidence of preferential dislocation accumulation and pileup at the surface as compared to the bulk. It was shown further that this surface layer also formed in commercial alloys during push-pull fatigue.[13,14] The long range stresses introduced as a result of the surface layer formation were considered to influence to a large degree the dislocation multiplication and interaction in the bulk. In the present investigation, a method based on X-ray double-crystal diffractometry (DCD) combined with Berg-Barrett (B-B) X-ray topography[15-17] was employed to disclose the excess dislocation density generated at the surface and in the bulk of deformed single crystals, or in the surface and bulk grains, respectively, of fatigued Al 2024 specimens.

In applying the DCD method a highly parallel, crystal-monochromated X-ray beam is used to impinge on the crystal specimen (or grains in polycrystalline materials). By rotating the specimen

R. N. PANGBORN, formerly Research Associate, Rutgers College of Engineering, is now Assistant Professor, Department of Engineering Science and Mechanics, The Pennsylvania State University, University Park, PA 16802, S. WEISSMANN is Professor, Department of Mechanics and Materials Science, College of Engineering, Rutgers University, Piscataway, NJ 08854, and I. R. KRAMER is Technical Advisor, Materials, David W. Taylor Naval Ship R&D Center, Annapolis, MD 21402.

Manuscript submitted November 26, 1979.

the reflecting (hkl) plane of the crystal (grain) is carried through the reflecting range and the reflected intensities are recorded as a function of crystal rotation. A rocking curve is thus obtained and the width at half the maximum intensity provides a measure of the lattice misalignment introduced during deformation to a single crystal or to the individual grains of a polycrystalline metal. If the rocking curve profile is smooth, its width may be interpreted in terms of the lattice distortions caused by strain or the formation of very fine substructure. In this case, a homogeneous distribution of dislocations of one sign in excess of the number having opposite sign would exist, with dislocations of each sign, positive and negative, randomly interspersed. If, on the other hand, the intensity fluctuates with the reflection angle, 2θ, so as to produce a multipeaked profile, the excess dislocations may be considered to be heterogeneously distributed, with local accumulations of the same sign giving rise to distinct lattice tilts. The angle between the subpeaks of such rocking curves would then represent the relative misorientation of adjacent lattice domains or subgrains which are separated by the tilt boundary, whereas the widths of well-resolved subpeaks indicate the degree of lattice distortion within the subgrains.[15] When the rocking curve widths or peak-to-peak angles are reasonably consistent for all the grains sampled by the incident beam, these parameters may be averaged independently to obtain a statistical evaluation of the damage induced in the region analyzed.

The information afforded by the DCD rocking curves is nearly equivalent to that furnished by the line-breadths from scanning diffractometry. The latter method was also used in this study to supplement the DCD method. Unlike the DCD method, however, conventional line broadening analysis provides a direct average of the deformation induced in all the grains intercepted by the incident X-ray beam. When the subgrain or cell size is less than about 0.5 μm, the relative contributions of the "particle" size and strain effects can be determined either by assuming distribution functions representative of each effect or by deconvolution of the line profiles using Fourier methods.[18,19] However, when scanning diffraction procedures are utilized the inhomogeneity of deformation in the individual grains cannot be analyzed nor topographically displayed, as in the case with the DCD method, supplemented by B-B topography.

Surface topographical features may also influence the shape of rocking curve profiles obtained by the DCD/B-B method. Figure 1 illustrates schematically the effect of particular deformation characteristics on the distribution of reflected intensity. Those grains that are affected by intense multiple slip activity (*a*), or grains located in the vicinity of microcracks (*b*), or grains subjected to both these effects (*c*) exhibit large angular misorientations. Even grains further removed from such localized strain centers "feel" sensitively the transmitted strain effects, which in turn are manifested by a commensurate increase of the rocking curve width. On the other hand, grains located deeper in the bulk (*d*) are only slightly affected by the transmitted strains and their rocking curves show a smaller degree of broadening.

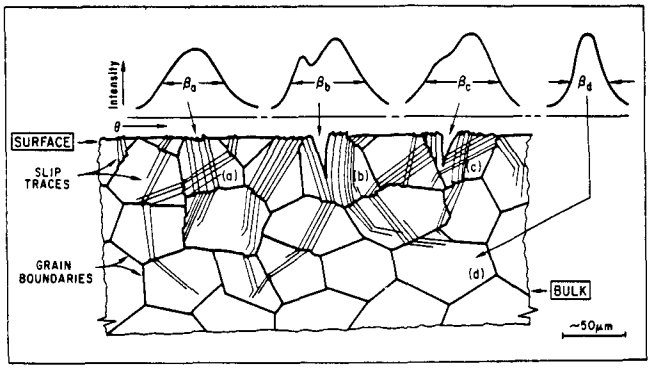

Fig. 1—Correlation of X-ray rocking curve half-widths to surface topographical features induced by fatigue: (*a*) rocking curve of grain with intense multiple slip activity, (*b*) effect of microcrack formation within persistent slip band on rocking curve, (*c*) rocking curve of grain with combined effects of (*a*) and (*b*): broad, asymmetrical line profile, (*d*) rocking curve for bulk grains far removed from strain centers.

2. EXPERIMENTAL PROCEDURE

2.1 Specimen Preparation and Mechanical Testing

Single-crystal specimens of silicon, aluminum and gold were prepared for simple tensile deformation to determine whether the observations from the X-ray analysis agreed with those obtained from methods analyzing their mechanical behavior. The aluminum (99.999 pct) and silicon shoulder-type specimens with gage sections about 20 mm long, 5 mm wide, and 1 mm thick were made by the Servomet spark-erosion technique. The silicon specimens had a $(1\bar{1}2)$ surface orientation and a [110] tensile axis. The surface orientation and tensile axis of the aluminum specimens were (010) and [100], respectively. The tensile axis for the gold was nearly $[\bar{1}23]$ and the (311) planes were oriented at an angle of about 11 deg to the surface of the square-section specimen (50 × 3 × 3 mm).

The surface damage was removed from the specimens by polishing electrochemically a layer of about 140 μm from the diameter thickness.[20] The aluminum specimens were annealed at 600 °C for 20 h in argon to relieve internal stresses introduced during preparation. The silicon specimens were strained 10 pct at 650 °C in argon at a strain rate of $5.9 \times 10^{-5} s^{-1}$. The aluminum specimens were mounted in a ball-bearing holder to prevent twisting during the deformation and strained 10 pct at a rate of $3.3 \times 10^{-3} s^{-1}$ at 0 °C. After straining, the specimens were held at −5 °C to prevent possible relaxation. The gold specimen was deformed 3 pct at a rate of $1.7 \times 10^{-5} s^{-1}$.

For the fatigue studies, cylindrical specimens with a gage length of 10 mm and diameters of 4.5 and 3.0 mm for the aluminum single crystals and Al 2024-T3 specimens, respectively, were cycled at 15 Hz in stress-controlled tension-compression ($R = -1$).

The dislocation concentration and distribution as a function of distance from the free surface of the deformed specimens were obtained by incrementally removing the surface layers and performing X-ray dif-

fraction analysis at each depth. The layers were polished away with the same chemical or electropolishing procedure used for each of the crystal species in the damage-removal step.

2.2 X-Ray Diffraction Procedures

X-Ray double-crystal diffractometry was employed as the principal research tool for the analysis of the dislocation structure induced by monotonic and cyclic testing. Both single and polycrystalline specimens could be studied by using counter and film methods, respectively, to record the diffraction patterns. For investigations involving incremental removal of the surface layers of deformed silicon crystals, Lang transmission topography was also employed (Fig. 2).

A dislocation-free silicon crystal with a (111) surface orientation was used as the first, monochromating crystal in the DCD arrangement. The K_{α_2} component of the reflected radiation was removed with a knife edge so that rocking curves such as those shown in Fig. 3 could be obtained either in transmission or reflection without interference from the K_{α_2} diffraction peak.

When polycrystalline specimens were studied, the individual grains were considered to function independently as the second crystal of a DCD. Rocking curves for the reflecting grains were obtained by irradiating the specimen with crystal-monochromated radiation and by recording the spot reflections on a cylindrical film along the Debye-Scherrer arcs. By carrying out incremental specimen rotations, combined with film shifts to separate the spot contributions, arrays of spots were obtained such as those shown in Fig. 6. The intensity dependence of each spot array represents the rocking curve for the grain. The width of each rocking curve at half the peak intensity maximum is denoted by the measured half-width, β_m. For patterns recorded in this investigation, the minimal variation in half-widths for grains reflecting to different (hkl) arcs indicated a nearly isotropic deformation response. Until fatigue cracks were initiated at a late stage in the life, grains with the same (hkl) reflection orientation also gave similar measured half-widths. Thus, the half-widths for all the grains intercepted by the incident X-ray beam could be averaged to give a representative half-width, $\bar{\beta}_m$, for the grain population in that sample region. This value was then corrected for the intrinsic half-width of the annealed and polished, virgin specimen, β_0, using a Gaussian reduction function of the form, $\bar{\beta} = (\bar{\beta}_m^2 - \beta_0^2)^{1/2}$, where $\bar{\beta}$ is the corrected average half-width.

The X-ray analyses of the silicon and gold monocrystals were performed at ambient temperature. The aluminum single crystals were mounted on a copper cooling block fitted to the diffractometer goniometer head. The temperature during X-ray analysis, measured by attaching a thermocouple to the grip section of the specimen, was maintained at 3 to 5 °C by a flow of ice water pumped through the cooling block. The maximum penetration of the Cu K_{α_1} radiation was estimated to be 24, 14, and 0.7 μm for the silicon, aluminum, and gold, respectively. For the Lang transmission topography of silicon crystals, Ag K_{α_1} radiation was employed.

2.3 Spectrum Loading Studies

An Al 2024 fatigue specimen was also tested under variable amplitude conditions. The fatigue sequence consisted of four blocks of cycling, each conducted at constant amplitude, zero mean stress, but at successively higher amplitude, followed by cycling to failure at the amplitude value of the last block. The number of cycles to failure during the final step was used in conjunction with the S-N curve to determine the fraction of life remaining after the fourth cycling block.

The specimen was analyzed by DCD utilizing Mo K_α radiation to obtain an average half-width value at

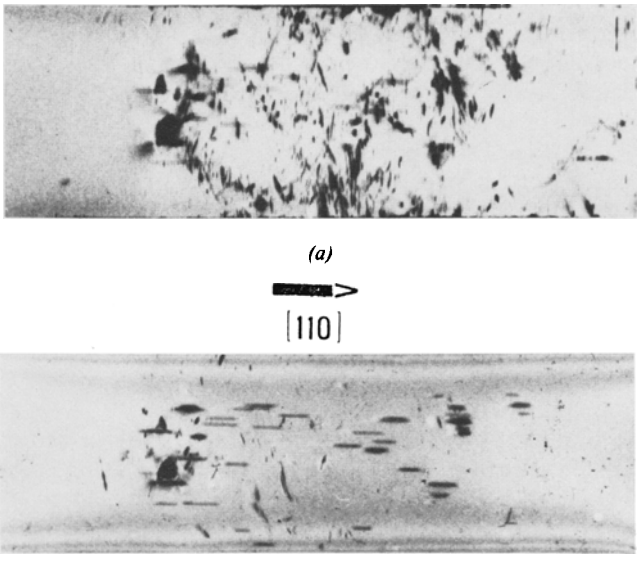

Fig. 2—Traverse X-ray topographs of flat silicon specimen deformed in tension at 800 °C, showing distribution of microplastic zones. Ag K_{α_1}, (200). (*a*) Without surface removal, (*b*) surface removal of 125 μm.

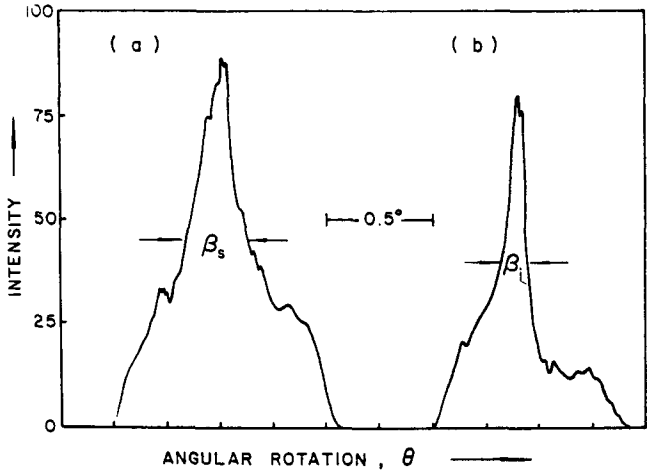

Fig. 3—X-ray rocking curve profiles of tensile deformed silicon single crystal. ϵ_{pl} = 10 pct, 650 °C, tensile axis [110], $(1\bar{1}2)$ reflection, Cu K_{α_1}. (*a*) Original surface, (*b*) after removal of a 100 μm surface layer.

the end of each cycling block. A planar region, 2 mm in width and 5 mm in length, was prepared by spark erosion along the gage section of the sample prior to final electropolishing and testing. The (111), (200), (222) and (400) line profiles were then recorded for this region after each block of the spectrum fatigue sequence by conventional scanning diffractometry. These line-broadening analyses were conducted using Zr-filtered Mo K_α radiation, and the $K_{\alpha_1}/K_{\alpha_2}$ doublet separation was accomplished according to the Rachinger correction.[21]

2.4 Calculation of Dislocation Density

It is generally accepted that an increase in the rocking curve half-width can be correlated to an increase in excess dislocation density. Since relatively smooth rocking curve profiles were obtained in this investigation for the tensile-deformed and fatigued samples, either single or polycrystalline, a predominance of the distortion effect over subgrain formation could be presumed. A model proposed by Hirsch[22] was adopted to describe the lattice distortion, for which the dislocations are considered to be randomly distributed so that there is a 50 pct chance for two dislocations of the same sign being adjacent to one another. If the normals of the very fine substructure causing the lattice distortion are distributed about a mean position according to a Gaussian function, the density of excess dislocations of one sign, ρ, may be calculated from the relationship:

$$\bar{\rho} = \bar{\beta}^2/9\mathbf{b}^2, \qquad [1]$$

where $\bar{\beta}$ is the average corrected half-width, and **b** is the magnitude of the Burgers vector.

The line-breadths recorded by scanning diffractometry were analyzed by the integral breadth method.[18] For consistency with the dislocation density calculations from the DCD data, Gaussian-Gaussian or Cauchy-Gaussian distributions were chosen to represent the profile shapes of the particle size and strain components, respectively. Since the results for either combination of assumed distributions were nearly identical, only those for the latter will be reported. For the Cauchy-Gaussian case, then, the parabolic relationship between the broadening due to particle size, B_D, and the strain broadening component, B_ϵ, is given by $B_\epsilon/B = 1 - (B_D/B)^2$, where B is the measured line-breadth, corrected for the intrinsic breadth of the virgin specimen. If the Scherrer equation[23] is used to describe the particle size contribution and the pure strain component is defined by the expression derived by Stokes and Wilson,[24] the overall broadening may be expressed in the form:

$$(B^2/\tan^2\theta) = (K\lambda/D)(B/\tan\theta\sin\theta) + 16e^2, \qquad [2]$$

where θ is the diffraction angle, λ is the wavelength, K is related to the particle shape and normally taken as unity, D is the particle size, and $e = (\Delta d/d)_{hkl}$ is the upper limit of the lattice distortion. The root-mean-square (rms) strain $\langle\epsilon^2\rangle^{1/2}$, is given by $e/1.25$.[24] A linear dependence may be obtained by plotting $(B^2/\tan^2\theta)$ against $(B/\tan\theta\sin\theta)$ for two or more orders of a particular (hkl) reflection. The slope of the line is inversely related to the particle size, while the strain may be evaluated from the intercept. Finally, these results may be interpreted in terms of the dislocation densities inherent to each effect. According to Cohen,[25] the dislocation density due to rms strain is given by $\rho_\epsilon = 12\langle\epsilon^2\rangle^{1/2}/\mathbf{b}^2$, and the dislocation density associated with the formation of substructure is $\rho_D = 1/D^2$. The geometric mean of the dislocation density for the two effects combined is $\bar{\rho} = (\rho_\epsilon\rho_D)^{1/2}$. It should be noted that since the absolute values of the dislocation density will vary considerably with the method selected for their evaluation, it is the relative change in dislocation density during or resulting from deformation that is of primary interest.

3. RESULTS

3.1 Preferential Deformation of Surface Layer and Depth Dependence of Deformation

Since silicon crystals can be obtained dislocation-free and have been shown to respond to plastic deformation at elevated temperatures in a fashion completely analogous to metal crystals,[26] they were investigated first. The X-ray diffraction analyses were subsequently extended to include metal crystals.

When a smooth, flat silicon specimen was lightly deformed in tension at 800 °C with an applied stress of 6.85 MPa, plastic zones were introduced. The surface layers were then systematically removed by chemical polishing and the character and change in distribution of the plastic zones were studied by Lang X-ray traverse (projection) topography. Fig. 2(*a*) shows the distribution of plastic zones without removal of surface material, while Fig. 2(*b*) exhibits the distribution after removal of 125 μm. Not only did the density of microplastic zones decline after removal of the surface layers, but the preferred alignment of the zones also shifted its direction. The preferred alignment at near-surface sites was perpendicular or inclined about 60 deg to the (110) tensile axis, while that in depth was parallel to the tensile axis. Topographs taken at intermediate depth levels showed a systematic change in both density and alignment. The 60 deg dislocations were conspicuously absent in the deeper layers of the crystal. The generation of these dislocations and of those pertaining to the primary slip system, $(\bar{1}11)[110]$, at or near surface sites, indicates that many dislocation reactions were possible at these sites, whereas in the bulk the possibility of these reactions was limited.[27,28]

When DCD was applied to study an undeformed silicon crystal, a typical half-width value for the rocking curve of about 15 s of arc was obtained. After 10 pct tensile deformation at 650 °C, the rocking curve profile developed shoulders as shown in Fig. 3(*a*), and the extent of the half-width, β, pertaining to the principal peak was 935 s of arc. Surface layers were removed by chemical polishing in steps of 30, 100, 175, and 250 μm. Fig. 3(*b*) shows the rocking curve

profile after removal of surface layers totaling 250 μm. Both the total range of reflection and the half-width decreased significantly. Figure 4 shows the gradient of excess dislocations obtained as a function of depth distance from the surface for silicon, a brittle material with low stacking fault energy when deformed at low temperature, *viz.* 650 °C; aluminum, a high stacking fault energy material; and gold, which exhibits very little or no propensity for formation of a surface oxide. For all three materials there was a decline by factors of 2.7 to 6.2 from a high surface dislocation density, $\bar{\rho}_s$, to a constant value, $\bar{\rho}_i$, at about 100 to 150 μm into the interior. Although tested to only 3 pct plastic strain, the gold revealed a similar gradient.

The distribution of excess dislocations in depth, indicated by the profile of measured half-widths, β, for aluminum crystals fatigued in axial tension-compression at a stress of ±1.03 MPa for 2×10^5 cycles is presented in Fig. 5. This stress is in the transition region between Stages I and II. Similar to the profile from monotonically deformed specimens, a decreasing gradient from the surface into depth, x, was produced by cycling. However, the β-x profile exhibits an additional salient feature. A minimum in the curve was obtained at a depth of 100 μm from the surface. Further in depth, the half-width values increased again and attained a plateau level at about 250 μm from the surface, which extended into the bulk. The β-values in the region from 25 to 150 μm were lower than the value of the virgin crystal, indicating that a redistribution of intrinsic dislocations occurred. For the core region of the specimen, no change in half-width from its intrinsic value was measured. Rocking curve analyses of the fatigue-induced dislocation structure were also carried out for Al 2024-T3. They were performed both as a function

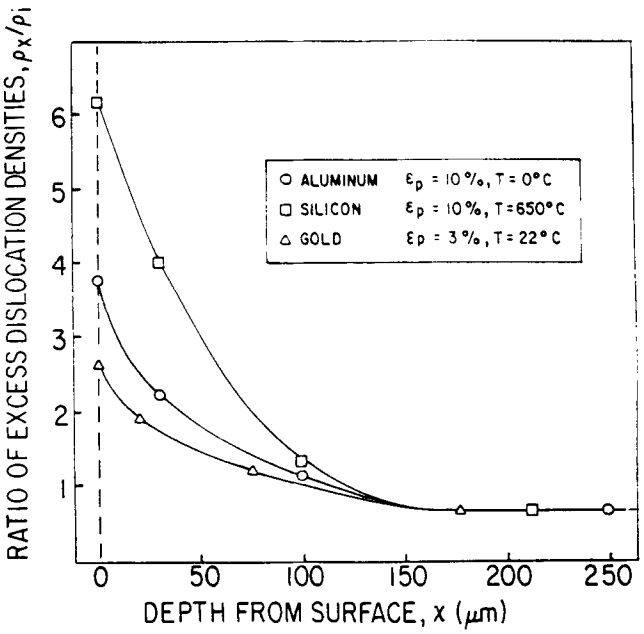

Fig. 4—Distribution of excess dislocations with depth from the crystal surface, expressed as the ratio of the density $\bar{\rho}_x$ at each depth to that of the bulk $\bar{\rho}_i$. Tensile axis and surface orientations: Al, <100> and (100); Si, <110> and (1$\bar{1}$2); Au, <$\bar{1}$23> and (311).

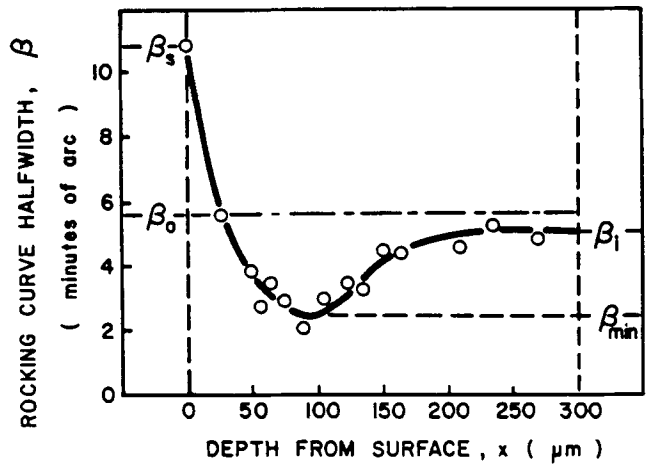

Fig. 5—Profile of the measured half-width dependence on depth from the surface for a fatigued Al single crystal: 2×10^5 cycles at ±1.03 MPa, <100>.

of the fraction of fatigue life, N/N_f, and as a function of the depth distance from the surface for fixed periods N/N_f of the life. The X-ray multiple exposure diagram of Fig. 6(*a*) gives a survey of the grain reflections and their rocking curves for a specimen fatigued 10^4 cycles. Figure 6(*b*) shows details of the rocking curve characteristics of some representative grains, giving clear evidence of the lattice distortion associated with the increase in excess dislocation density induced by fatigue. The progressive broadening of the rocking curve of an individual grain at various fractions of the fatigue life of an Al 2024 sample is shown in Fig. 6(*c*).

The data presented in Fig. 7, part *A*, were obtained from the rocking curve analysis of Al 2024-T3 specimens cycled for various fatigue life fractions at ±200 MPa, corresponding to the proportional limit. Analogous to the deformation characteristic of monotonically and cyclically stressed single crystals, the β-x profile revealed a higher excess dislocation density in the surface layer than in the bulk. Up to about 0.15 pct of the fatigue life (N_f = 21,000), the ρ-x profile was similar to that observed after simple tension. Observations made after 5 pct of the life showed that the dislocation density in the bulk also increased, and a trough appeared on the ρ-x profile in the subsurface region. With further cycling, the excess dislocation density continued to increase in the surface layer and in the bulk.

Figure 8 exhibits the ratio of the excess dislocation density in the bulk to that of the surface as a function of the fatigue life fraction for Al 2024 cycled at ± 200 MPa. At 0.05 N_f, ρ_i is only about 0.3 ρ_s. The ratio increases with cycling until 0.95 N_f, where ρ_i is about 0.7 ρ_s.

3.2 Instability of Fatigue-Induced Defect Structure of Bulk Material upon Removal of Surface Layer

To test the stability of the dislocation structure in the grains of the bulk induced by cycling, a further experimental program was carried out. As shown in the composite diagram of Fig. 7, the surface layers of

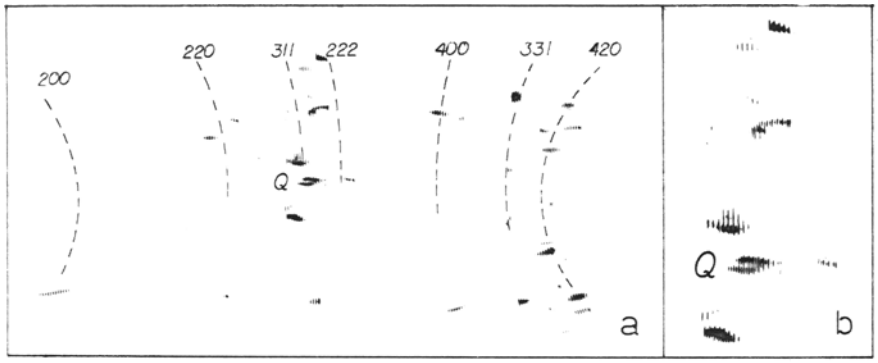

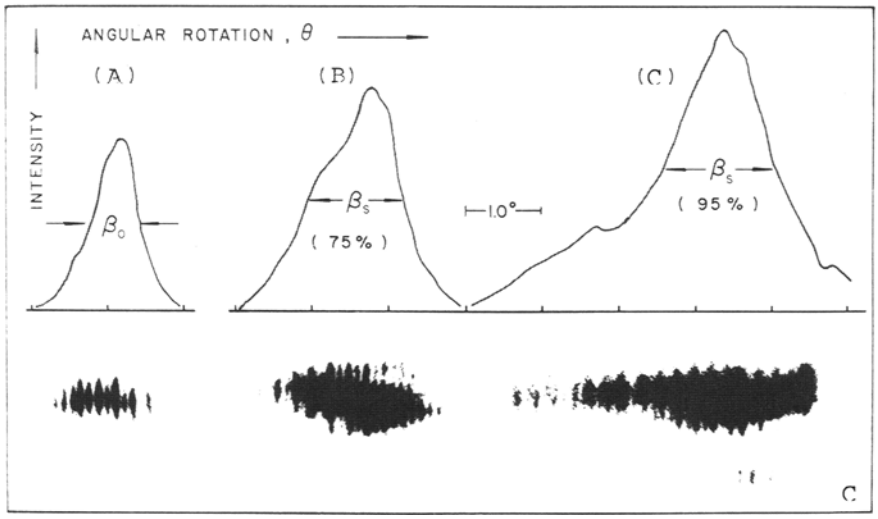

Fig. 6—Rocking curves for the grains of a polycrystalline specimen. (*a*) survey of grain reflections along Debye-Scherrer arcs for an Al 2024 specimen fatigued 10^4 cycles at ±100 MPa, (*b*) detail of spot arrays for grains *Q*, obtained by discrete specimen rotations of 6 min of arc, accompanied by appropriate film shifts, (*c*) rocking curves obtained microphotometrically for grain reflections recorded on film during controlled specimen rotation at various stages of the fatigue life at ±200 MPa. (*A*) annealed and undeformed, (*B*) cycled to 0.75 N_f, (*C*) cycled to 0.95 N_f.

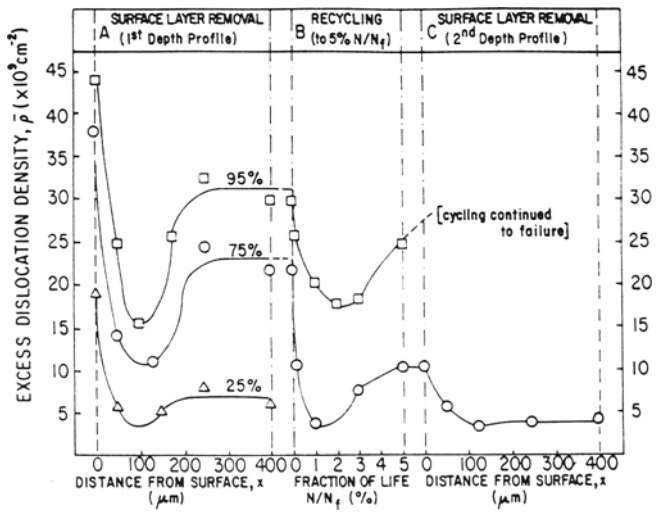

Fig. 7—Composite diagram for Al 2024 specimens given prior fatigue to 75 and 95 pct of their life at ±200 MPa, followed by surface removal (part *A*) and recycling (part *B*), and either continued recycling or X-ray analysis in depth (part *C*).

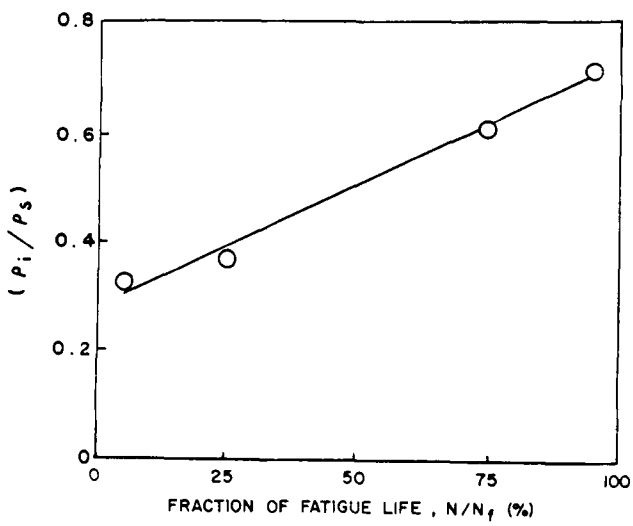

Fig. 8—Ratio of excess dislocation density in the bulk, ρ_i, to that at the surface, ρ_s, as a function of fatigue life for Al 2024 cycled at ±200 MPa.

previously cycled specimens were removed by electropolishing to a depth of 400 μm. The specimens given prior cycling to 75 to 95 pct of their life, followed by surface removal, were then reinserted in the fatigue equipment for continued cycling at the same amplitude. The excess dislocation density declined rapidly during the initial cycles of renewed fatigue, as revealed in part *B* of the figure. This behavior can be attributed to the instability of the bulk dislocation structure on initial cycling when the work-hardened

surface layer was absent. After reaching a minimum at 1 to 2 pct of the life, the density began to increase again at approximately the same rate as in the original fatiguing.

When the cycling process was again interrupted after 5 pct to obtain a second depth profile, as exhibited in Fig. 7, part *C*, analysis of the specimen given 75 pct prior cycling revealed an excess dislocation density which, with the exception of the immediate surface, was uniform over the entire cross section and nearly equal to the value of the undeformed, virgin specimen. The instability of the bulk dislocation structure when cycling is resumed after elimination of the work-hardened surface contributes to the extension of fatigue life afforded by judicious, periodic surface layer removal.[29,30] It is to be noted that at 75 pct of the life, virtually no surface markings due to fatigue could be observed by optical or scanning electron microscopy, nor were microcracks detected for specimens cycled to 0.95 N_f. When a specimen that was first cycled to 95 pct of its life, was subsequently polished to 400 μm in depth and then fatigued to failure without interruption, a 75 pct net increase in its normal fatigue life was obtained.

3.3 Three-Stage Development of Dislocation Density in Fatigued Surface Layer

Figure 9 shows data from X-ray analyses of the surface layer using shallow-penetrating Cu K_α radiation, after cycling to various fractions of the fatigue life. The results are plotted for specimens with two average grain sizes, differing by about 25 pct in grain diameter, and for tests carried out at two different stress amplitudes. In agreement with the findings of Taira *et al*[31,32] the change in dislocation density during the life could be described by a three-stage sequence for all the tests. Rapid increases in the dislocation concentration occurred early (Stage I) and late (Stage III) in the life. A markedly shallower slope was obtained for the long duration of the second stage, comprising the period from 0.15 to 0.95 N_f. All the data fell within the experimental error band, even for the alternate grain size stock if a uniform shift factor related to the grain diameters was applied.[33] The appearance of surface markings induced by fatigue was observed by optical microscopy only for specimens cycled to Stage III.

3.4 Determination of Fatigue Damage

Of interest in Fig. 9 is the observation that all the points fall on a single curve independent of the stress amplitude and compensated for grain size. Most importantly, a propagating crack is apparently initiated and failure occurs when a critical value of the excess dislocation density, ρ^*, of 1.45×10^{14} m^{-2} is attained. It is evident that if ρ^* can be determined, and the relationship between fatigue damage and the excess dislocation density is established, an assessment of the fatigue damage can be made. It may be concluded from Fig. 9, as well as from the data of Taira *et al*,[5,6,31,32] that the slope of Stage II is too low to be used for accurate and practical determination of fatigue damage. An examination of the depth profiles shown in Fig. 7(*a*) reveals that the buildup of the dislocation density at the surface occurs much earlier in the life than in the bulk. However, inspection of the plateau values established at about 250 μm discloses that the average excess dislocation density in the bulk increases steadily throughout the life. It follows that the fatigue damage can be determined provided that the X-ray beam penetrates sufficiently far into the material to sample both the surface layer and bulk. Experimentally, this can be achieved by application of X-rays with short wavelength, such as Mo K_α radiation. Figure 10

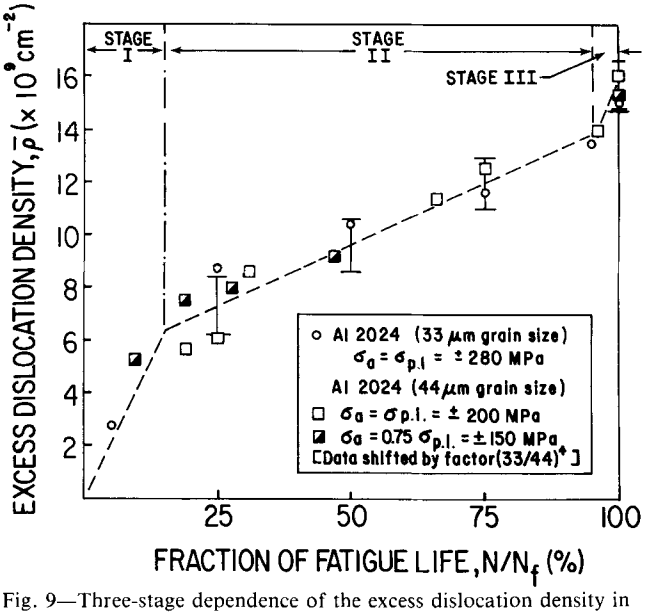

Fig. 9—Three-stage dependence of the excess dislocation density in the surface layer during the fatigue life for two Al 2024 batches, tested at various amplitudes.

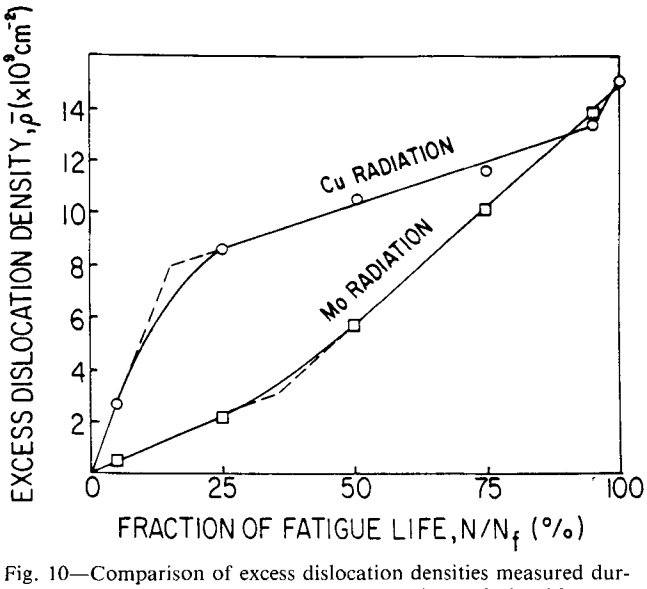

Fig. 10—Comparison of excess dislocation densities measured during the fatigue life of Al 2024 at ±280 MPa by analysis with copper and molybdenum radiation.

exhibits a plot which compares the average excess dislocation densities obtained by measurements with copper and molybdenum radiation. It can be seen that by applying molybdenum radiation, a sharp incline of the slope is obtained up to the critical value ρ^*, which enables one to determine the accumulated damage unequivocally. By contrast, application of copper radiation which samples only the dislocation density in the quickly saturated surface layer does not provide an accurate evaluation of cumulative damage or of expended fatigue life, owing to the shallow slope during the intermediate life fractions.

3.5 Line Broadening for Variable Amplitude Fatigue

For the spectrum fatigue studies of Al 2024, a sequence of cycling blocks as shown in Fig. 11 was selected. The number of cycles at each amplitude was chosen with reference to the S-N curve to represent approximately equal increments in terms of the fraction of fatigue life. In the figure, the X-ray data is expressed in the form of normalized rocking curve half-widths, denoted by the ratio of the average measured half-widths, β_m, to the intrinsic half-width for the undeformed specimen, β_0. The solid line gives the dependence of the normalized half-widths on the fraction of life for the Al 2024 specimens previously analyzed with Mo K_α radiation during constant amplitude fatigue. It may be regarded, therefore, as the reference standard curve. The total increase in half-width during the life, indicated by the critical half-width ratio at failure, $(\bar{\beta}_m/\beta_0)^*$, was found to be almost a factor of two. The normalized rocking curve half-widths measured after each cycling block of spectrum fatigue are plotted along this curve. The number of cycles to failure recorded for uninterrupted fatiguing after the fourth block was 3.19×10^3, or about 42.5 pct of the total lifespan under constant amplitude fatiguing. This value for the remaining life is highly consistent with the direct estimate of the remaining life fraction furnished by the X-ray data after the fourth cycling block. In conjunction with the previously generated calibration curve (solid line), the expended life at this point can be approximated at 54 pct, leading to an estimate for remaining life of about 46 pct.

The line-breadths of the (111), (200), (222) and (400) diffraction lines, obtained by a conventional diffractometer scan using Mo K_α radiation, were also recorded after each cycling block. The data for each stage in the life was plotted according to Eq. [2]. Then, by plotting the intercept of each line against the corresponding fraction of life determined for each block from Fig. 10, a linear dependence was obtained that could be extrapolated to 100 pct. The critical rms strain at failure could be computed as about 7.5×10^{-3}. The slopes of the linear plots constructed from Eq. [2] were used to calculate the particle size at each fraction of life. This parameter was nearly invariant during the life, with an average value of about 0.0230 μm.

4. DISCUSSION

4.1 Role of the Surface Layer in Deformation Processes

The X-ray analysis of the dislocation structure induced in various materials by monotonic and cyclic deformation have shown that the surface layer exhibits a special propensity for work hardening. It has been demonstrated further that mechanical deformation generates a gradient of the density of excess dislocations of one sign from the surface into the bulk material (Figs. 4, 5, 7–9). These results are in agreement with previous investigations of Kramer,[9,10,13,14,34] who studied the role of surface layer stress in deformation processes. The surface layer stress was defined as the additional stress opposing the motion of dislocations due to preferential work hardening in the surface layer.

It is interesting to note that the distribution of the excess dislocation density with depth from the surface for the tensile-deformed monocrystals, as shown in Fig. 4, is remarkably similar to that reported by Belykh *et al*[35] for ground alkali halide crystals. The relationship proposed by Belykh *et al* may be written as

$$ln[(\bar{\rho}_x/\bar{\rho}_i) - 1] = ln\,[(\bar{\rho}_s/\bar{\rho}_i) - 1] - kx, \qquad [3]$$

where $\bar{\rho}_s$ is the dislocation density at the surface, $\bar{\rho}_i$ is the constant dislocation density established at some depth into the bulk, and $\bar{\rho}_x$ is the dislocation density at a distance x from the surface. The data for silicon, aluminum and gold are given in terms of Eq. [3] in Fig. 12. The slopes k for all three materials are the same ($k = 2.8 \times 10^4 m^{-1}$). Belykh *et al* reported values for k equal to 3.9×10^4 and $1.7 \times 10^4 m^{-1}$ for two NaCl crystals investigated.

The special propensity for surface work hardening is also a crucial factor in the case of fatigue cycling, which is known to be a highly surface-sensitive mode of deformation. Kramer postulated that a propagating fatigue crack was formed whenever the surface layer stress attained a critical value, particular to each material.[14] This value was independent of the stress amplitude, the testing environment, and the prior cyclic history. The X-ray diffraction analyses of the present study suggest that this critical value of the surface layer stress is directly associated with the critical value of the density of excess dislocations, ρ^*, in the surface layer (Fig. 9 and 10).

When the Al 2024 alloy was cycled at an amplitude below its fatigue limit, the increase in excess dislocation density was restricted to the surface layers, with no measurable change in dislocation structure occurring in the bulk. This surface layer effect was completely analogous to the deformation behavior depicted by Fig. 5 for single crystals fatigued 2×10^5 cycles at a low stress amplitude in the Stage I to Stage II transition region. Although the applied stress exceeded the critical resolved shear stress (CRSS) of the primary slip system, no increase in the excess dislocation density for the interior, computed from β_i, was observed. The surface dislocation density, on the other hand, showed a four-fold increase, correspon-

ding to the half-width expansion from 5.5 min of arc before fatigue to 10.7 min after cycling. Tests of single crystals at higher stress amplitudes were prevented by the rigid mounting assembly required for tension-compression testing since the restriction of lattice rotation would produce erroneous results. When Al 2024 samples were tested at amplitude levels sufficiently high to cause eventual failure, however, the excess dislocation density increased throughout the specimen cross section. This is illustrated by the depth profiles presented in part *A* of Fig. 7. Consequently, it is postulated that the buildup of excess dislocation density in depth is a direct result of the continued work hardening of the surface layer during stressing above the fatigue limit.

The formation of a trough in the profile of the dislocation density from surface to bulk is also an interesting phenomenon. This feature was observed for both single crystal and Al 2024 fatigue specimens, located in the subsurface region extending from 50 to 200 μm in depth. Inspection of Fig. 7, part *A*, shows that the trough is retained throughout the life and becomes more pronounced with progressive cycling. It has also been observed for work in progress involving tension-tension fatigue of Al 2014-T4,[36] but is never produced during monotonic or static testing. This is illustrated by the simple decreasing gradients of the dislocation density from surface to bulk obtained for tensile-deformed single crystals (Fig. 4) and the results of ongoing stress-corrosion experiments on 304 stainless steel and α-Ti.[36] It is therefore apparent that the existence of the half-width minimum in the subsurface, and hence the elevation of the bulk half-widths to a higher plateau value, is a unique result of cyclic deformation. The distinction between the dislocation distributions in depth for the fatigued and tensile-deformed metals may well be related to differences in dislocation structure identified by Wilkens *et al* for cyclically and unidirectionally deformed copper single crystals.[37] These authors noted a predominance of primary edge-dislocation dipoles at the surface for fatigued specimens, accompanied by insignificant long range internal stresses. Tensile specimens, on the other hand, revealed a high surface density of secondary dislocations with significant long range stresses. Thus, the possibility exists that strain relaxation occurs in the transition region between the surface layer and the core for cycled specimens, which may be interpreted as a dynamical recovery facilitated by repeated stressing as compared to static loading. Once formed, the trough is maintained during subsequent cycling as the bulk region exhibits a steadily increasing dislocation density in response to the enhanced work hardening at the surface.

The experimental sequence protrayed by Fig. 7 provides evidence of the strong influence the surface layer exerts on the development of the bulk dislocation structure during the life. Fig. 7, part *B*, reveals a dramatic reduction in the bulk excess dislocation density when the specimens were subjected to renewed fatigue after removal of the surface layer produced by prior cycling. If the bulk dislocation structure did not depend on the surface layer, an increase in excess dislocation density would have been expected when the cycling was resumed. To the contrary, however, a dynamic recovery, evidenced by the decreasing average dislocation density for the sampled grains occurred throughout the specimen (Fig. 7, part *C*). Only after cycling beyond 2 to 3 pct of the normal life did the excess dislocation density begin to increase again as a new surface layer was being formed. The nature of the relaxation or recovery mechanisms responsible for this behavior will be a subject of future study.

The dislocation distribution in fatigued single crystals and polycrystalline samples, and the changes observed for the interior of Al 2024 specimens during fatiguing after surface removal, all show convincingly that during cycling the dislocation multiplication in the bulk is controlled by the surface layer. Since the stresses required to activate dislocation sources in the interior are larger than those required for surface or near surface sources,[38,39] it follows that the stress fields from the dislocations in the surface layer act over long distances to actuate sources throughout the bulk of the specimen. The net stress in addition to the applied stress which acts on the interior dislocation sources is, accordingly, a function of the stress fields associated with dislocations in the surface layer. Thus, elimination of the surface layer introduced by prior fatigue actually promoted a reduction in accrued damage during subsequent cycling. When Al 2024 was treated in this manner a large extension of the normal life was achieved.

This behavior appears to be related to the decline in work hardening rates observed for metals stressed in a solution containing surface agents,[40] in vacuum,[41] and under conditions where the surface layer is removed continuously during the stressing operation.[9] In all three cases, the extent of Stage I and Stage II for single crystals increases, the slopes decrease, and the flow stress in Stage III as well as the flow stress in polycrystalline materials is reduced. If the work hardening of the bulk is affected by the behavior of the surface under the imposed environmental condition, then the "softening" may be ascribed, not to the surface layer alone, but rather to the complementary reaction of the interior to the work hardening rate at the surface. It is proposed that, in general, the influence of the environment or coatings on the mechanical behavior can be described in terms of the response of the bulk material to the stress fields originating in the surface and changes in work hardening rates at the surface.

4.2 Dislocation Distribution in Surface and Bulk and Its Role in Forecasting Fatigue Failure

A remarkable aspect of the in-depth study of fatigue-indiced dislocation structures is the new perspective it provides on the problem of fatigue failure prediction. As mentioned previously, the X-ray line broadening investigations of fatigued materials have inevitably revealed rapid changes in the peak breadths very early in the life, with little change occurring during the intermediate life fractions. Thus,

these analyses of the evolution of a surface layer dislocation structure were insufficient with regard to failure prediction, nor could observations of the surface topography itself be used to estimate the time of, or potential for, failure. The present study of the distribution of the excess dislocations density from surface to bulk have disclosed that the surface layer dislocation density increases even for cycling carried out at low stress amplitudes. Therefore, measurements confined to the outer regions of the surface layer cannot be utilized as an indication of fatigue damage. The change in the bulk dislocation structure, on the other hand, although dependent on the work hardening at the surface, has been shown to occur more steadily over the lifetime of the cycled material. Thus, by applying deeply-penetrating radiation such as molybdenum for analysis of aluminum alloys, a steeper dependence of the excess dislocation density as a function of the life fraction is obtained. From this curve, shown in Fig. 10, the remaining life of the specimen may be accurately determined by comparison with the critical value ρ^*. The limited investigation of Al 2024 under spectrum fatigue conditions, for which results are given in Fig. 11, has indicated that this approach for estimating expended life is viable for more complex cyclic histories. For a sequence of cycling blocks with successively higher amplitudes, thereby avoiding the anomalous load interaction effects associated with overstressing or large decrements in stress amplitude, the direct estimation of remaining life from the X-ray data (46 pct) was accurate to within 10 pct of the fraction determined by cycling to failure (42.5 pct).

It appears that some of the great precision attained by applying the X-ray double-crystal diffractometer to analyze the fatigue-induced damage of the grains, can be traded for greater speed and a wider range of sampling by carrying out conventional diffractometer measurements. Such line broadening studies are being performed using Mo K_α radiation in the current spectrum fatigue investigation (Table I). The results thus far have provided a linear dependence of the rms strain, $\langle\epsilon^2\rangle^{1/2}$, on the fraction of life, and a nearly invariant particle size averaging 0.023 μm. The critical value of the dislocation density may be obtained for the strain component, extrapolated to 1.0 N_f, of 7.5×10^{-3} using the appropriate formula of Cohen,[25] which which results in a computed value of $\rho_\epsilon = 8.23 \times 10^{15}\text{m}^{-2}$. Employing the Cohen relationship for the dislocation density due to the particle size, a value of $\rho_D = 1.89 \times 10^{15}\text{m}^{-2}$ is calculated. The mean dislocation density resulting from the two contributions to the overall broadening is then given by $\bar{\rho} = (\rho_\epsilon \rho_D)^{1/2} = 3.94 \times 10^{15}\text{m}^{-2}$. Although none of these values should be taken as absolute or peremptory since they depend on the particular experimental and analytic methods used in their evaluation, they do provide a quantitative measure of fatigue damage when used consistently. For purposes of comparison, the critical half-width at failure of 36 min of arc measured by DCD may be assumed to be related entirely to lattice strain. Substituting this value for β_ϵ in the pure strain broadening equation, $\beta_\epsilon = 4e\tan\theta$, and using the Stokes-Wilson[24] conversion to rms strain, result in a calculated value for $\langle\epsilon^2\rangle^{1/2}$ of 8.0×10^{-3}. This

Table I. Calculated Dislocation Densities at Failure for Spectrum Fatigue of Al 2024

Double Crystal Diffractometry	
Critical Excess Dislocation Density Calculated from Rocking Curve Half-widths	$\rho^* = 1.45 \times 10^{14}\text{m}^{-2}$
Scanning (Powder) Diffractometry	
Critical Dislocation Density Due to Strain Component of Line-breadths ($\langle\epsilon^2\rangle^{1/2} = 7.5 \times 10^{-3}$)	$\rho_\epsilon = 8.23 \times 10^{15}\text{m}^{-2}$
Critical Dislocation Density Due to Particle Size Component of Line-breadths ($D = 0.0230\ \mu$m)	$\rho_D = 1.89 \times 10^{15}\text{m}^{-2}$
Geometric Mean of Strain and Particle Size Contributions	$\bar{\rho} = 3.94 \times 10^{15}\text{m}^{-2}$

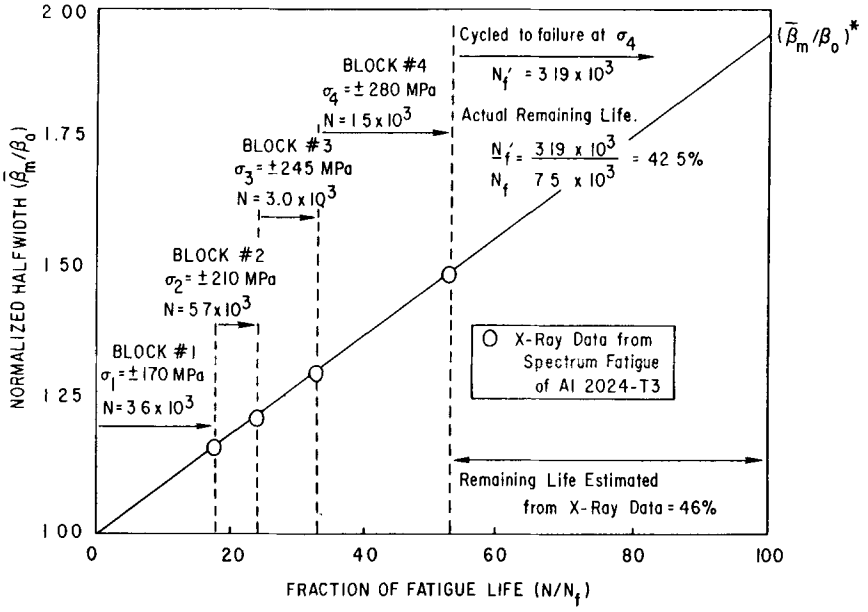

Fig. 11—Normalized rocking curve half-widths after each block of spectrum fatigue plotted along calibration curve from prior constant-amplitude cycling of Al 2024 at ±280 MPa.

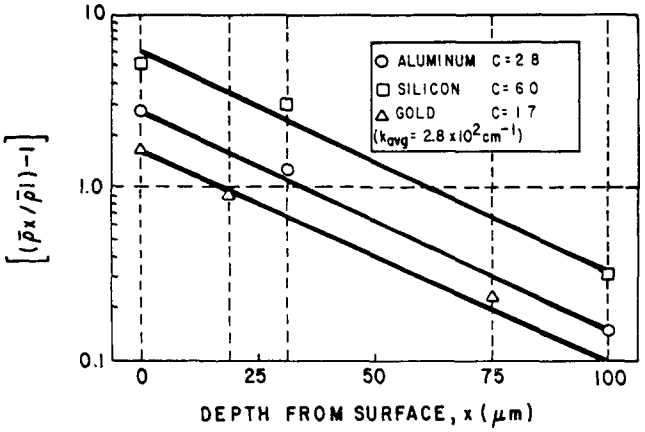

Fig. 12—Comparison of the linearized excess dislocation density gradients from surface to bulk for tensile-deformed Si, Al, and Au monocrystals.

magnitude of strain is in very good agreement with the rms strain contribution of 7.5×10^{-3} determined from the line-breadths. It may be concluded, therefore, that a reasonable correlation exists between the structural information afforded by the DCD and scanning diffraction techniques, respectively.

It is interesting to compare the dislocation density $\bar{\rho} = 4 \times 10^{15} m^{-2}$ obtained in this study for cycled 2024 Al with the dislocation densities recently obtained by Wilkens *et al*[37] who analyzed the X-ray profiles of cyclically deformed copper crystals applying resolved shear stresses of 30 MPa. These authors differentiated between the dislocation density of the matrix and that of the persistent slip bands (PSBs). They obtained for the total dislocation density the values of $8.5 \times 10^{14} m^{-2}$ and $5.6 \times 10^{14} m^{-2}$ for the matrix and PSBs, respectively. Calculating the local dislocation densities, ρ_{loc}, in the veins of the matrix and in the walls of the PSBs they obtained values of $1.28 \times 10^{15} m^{-2}$ and $6.3 \times 10^{15} m^{-2}$, respectively. With the aid of these values they computed a mean spacing from dipole to dipole of 0.14 μm in the walls of the PSBs and about 0.40 μm in the veins of the matrix. A very recent study of Winter[42] who investigated the dislocation structure in the interior of a fatigued copper polycrystal by TEM, applying an axial plastic strain amplitude of $\pm 1.25 \times 10^{-3}$ obtained evidence that after 12×10^3 cycles the interior was filled with PSBs. The wall structure appeared to occupy almost the whole of the polycrystalline sample and the wall spacing was 0.6 μm, markedly different from that found in single crystals (1.38 ± 0.05 μm). It will be noted that the $\bar{\rho}$ value of the present study may be regarded as an average of ρ_{loc} in the veins of the matrix and the walls of the PSBs computed by Wilkens *et al.* Since in the bulk of cycled polycrystalline samples the dislocation structure appears to be made up regularly disributed PSBs,[42] it is suggested that the particle size of the 0.0230 μm obtained in this study can be regarded as the average size of coherently diffracting lattice domains, and consequently may be related to the dipole separation distance.

5. SUMMARY

The X-ray rocking curve investigations, coupled with reflection topography, were performed on tensile-deformed silicon, aluminum and gold single crystals, fatigue-cycled aluminum single crystals, and Al 2024-T3 alloy specimens subjected to constant amplitude cycling and spectrum fatigue. The following results were obtained:

1) For tensile-deformed single crystals, a work-hardened surface layer was formed that could be described quantitatively by a decreasing gradient in the density of excess dislocations of one sign from the surface to a depth of 100 to 150 μm into the bulk. This behavior agreed with previous results obtained by mechanical methods,[9,10,34] etch pit studies,[11] and TEM analysis.[12]

2) A special propensity for surface layer work hardening was also disclosed for aluminum single crystals and Al 2024 specimens subjected to tension-compression fatigue. After decreasing to a minimum value at about 100 μm in depth, the excess dislocation density increased again to a constant plateau level in the bulk material.

3) The dislocation structure and arrangement in the bulk were unstable when cycled in the absence of the surface layer. This contributed to the extension of fatigue life afforded by judicious surface layer removal.

4) The buildup of excess dislocations in the surface occurred early in the life, as shown also by previous X-ray line broadening analyses,[5,6,31,32] and henceforth this work-hardened layer controlled the dislocation multiplication in the bulk.

5) When a critical excess dislocation density, ρ^*, was exceeded, fracture occurred. Because the excess dislocation density in the bulk material of aluminum alloy samples rose steadily up to this critical value, the accrued fatigue damage at any stage of life could be determined using deeply-penetrating molybdenum radiation. Initial tests of Al 2024 in spectrum fatigue indicated that this approach for estimating the fatigue damage may be viable even when the cyclic history is unknown. For these experiments, the results of line broadening analyses by scanning diffractometry compared favorably with the rocking curve half-width data derived from double-crystal diffractometry.

ACKNOWLEDGMENT

The support of this work by the David W. Taylor Naval Ship Research and Development Center, Annapolis, Maryland, is gratefully acknowledged.

REFERENCES

1. C. S. Barrett: *Structure of Metals; Crystallographic Methods, Principles and Data*, 1st ed., p. 337, McGraw Hill Book Co., New York, 1943.
2. H. J. Gough and W. A. Wood: *Proc. Roy. Soc.* (London), 1936, vol. A154, p. 510.
3. R. G. Spencer and J. W. Marshall: *J. Appl. Phys.*, 1941, vol. 12, p. 191.
4. J. A. Bennett: *J. Res. NBS*, 1951, vol. 46, p. 457.
5. S. Taira and K. Hayashi: *Bull. JSME*, 1966, vol. 9, p. 627.

6. S. Taira, T. Goto and Y. Nakano: *Proc. 12th Jap. Congr. on Materials Research,* p. 8, The Society of Materials Science, Kyoto, 1969.
7. G. Koves: *Microstructural Science,* 1976, vol. 4, p. 233.
8. M. Nagao and V. Weiss: *Trans, ASME,* 1977, ser. H, vol. 99, p. 110.
9. I. R. Kramer and L. J. Demer: *Trans. TMS-AIME,* 1961, vol. 221, p. 780.
10. I. R. Kramer: *Trans. TMS-AIME,* 1964, vol. 230, p. 991.
11. G. Vellaikal and J. Washburn: *J. Appl. Phys.*, 1969, vol. 40, p. 2280.
12. T. Tabata and H. Fujita: *J. Phys. Soc. Jap.*, 1972, vol. 32, p. 1536.
13. I. R. Kramer: *Proc. Air Force Conf. on Fatigue,* 1969, AFFDL-TR-0-144.
14. I. R. Kramer: *Met. Trans.*, 1974, vol. 5, p. 1735.
15. S. Weissmann and D. L. Evans: *Acta Cryst.*, 1954, vol. 7, p. 733.
16. S. Weissmann: *J. Appl. Phys.*, 1956, vol. 27, p. 389.
17. S. Weissmann: *Trans. ASM,* 1960, vol. 52, p. 509.
18. H. P. Klug and L. E. Alexander: *X-Ray Diffraction Procedures For Polycrystalline and Amorphous Materials,* 2nd ed., p. 661, John Wiley and Sons, New York, 1974.
19. B. E. Warren and B. L. Averbach: *J. Appl. Phys.*, 1950, vol. 21, p. 595.
20. R. Strickler and G. R. Booker: Scientific Paper 63-148-546-P5, Westinghouse Res. Lab., Pittsburgh, PA, 1963.
21. W. A. Rachinger: *J. Sc. Intrum.*, 1948, vol. 25, p. 254.
22. P. B. Hirsch: *Prog. Met. Phys.*, 1956, vol. 6, p. 236.
23. P. Scherrer: *Gött. Nachr.*, 1918, vol. 2, p. 98.
24. A. R. Stokes and A. J. C. Wilson: *Proc. Phys. Soc.* (London), 1944, vol. 56, p. 174.
25. J. B. Cohen: *Diffraction Methods in Materials Science,* p. 315, Macmillan Co., New York, 1966.
26. H. Alexander: *Z. Metallk.*, 1961, vol. 52, p. 344.
27. S. Schafer: *Phys. Stat. Sol.*, 1967, vol. 19, p. 297.
28. V. N. Erofeev, V. L. Nikitenko, and V. B. Osvenskii: *Phys. Stat. Sol.*, 1969, vol. 35, p. 79.
29. N. Thompson, N. Wadsworth, and N. Louat: *Phil. Mag.*, 1956, vol. 1, p. 113.
30. I. R. Kramer and A. Kumar: *Met. Trans.*, 1972, vol. 3, p. 1223.
31. S. Taira and K. Hayashi: *Proc. 9th Jap. Congr. on Testing Materials,* p. 1, The Society of Materials Science, Kyoto, 1966.
32. S. Taira, K. Tanaka, and T. Tanabe: *Proc. 13th Jap. Congr. on Materials Research*, p. 14, The Society of Materials Science, Kyoto, 1970.
33. S. Weissmamn, R. Pangborn, and I. Kramer: *Fatigue Mechanisms,* p. 163, ASTM STP 675, 1979.
34. I. R. Kramer: *Trans. AIME*, 1965, vol. 233, p. 1462.
35. G. I. Belykh, G. M. Pyatigorskiĭ, and E. I. Raĭkhel's: *Sov. Phys. Sol. St.*, 1976, vol. 18, p. 161.
36. S. Weissmann, R. Yazici, T. Takemoto, T. Tsakalakos and I. R. Kramer: Report #ONR-R-2, Office of Naval Research, Arlington, VA, 1979.
37. M. Wilkens, K. Herz and H. Mughrabi: *Z. Metallkd.*, 1980, vol. 71, p. 376.
38. J. C. Fisher: *Trans. AIME*, 1956, vol. 194, p. 531.
39. K. Sumino: *J. Phys. Soc. Jap.*, 1962, vol. 17, p. 454.
40. P. A. Rehbinder and E. K. Wenstrom: *Byull, Akad. Nauk. URSS,* 1937, *Classe Sci. Mat. Sea. Phys.*, p. 531.
41. I. R. Kramer and S. Podlaseck: *Acta Met.*, 1963, vol. 11, p. 70.
42. A. T. Winter: *Acta Met.*, 1980, vol. 28, p. 963.